

Geochemistry, Geophysics, Geosystems

RESEARCH ARTICLE

10.1002/2015GC006002

Key Points:

- Meteoric diagenesis in the mid-Carboniferous is a global phenomenon
- Meteoric diagenesis of carbonates can increase the $\delta^{13}\text{C}$ of the ocean
- This increase in ocean $\delta^{13}\text{C}$ is decoupled from organic carbon burial

Supporting Information:

- Supporting Information S1
- Data Set S1

Correspondence to:

B. Dyer,
bdyer@princeton.edu

Citation:

Dyer, B., A. C. Maloof, and J. A. Higgins (2015), Glacioeustasy, meteoric diagenesis, and the carbon cycle during the Middle Carboniferous, *Geochem. Geophys. Geosyst.*, 16, doi:10.1002/2015GC006002.

Received 9 JUL 2015

Accepted 9 SEP 2015

Accepted article online 14 SEP 2015

Glacioeustasy, meteoric diagenesis, and the carbon cycle during the Middle Carboniferous

Blake Dyer¹, Adam C. Maloof¹, and John A. Higgins¹

¹Department of Geosciences, Princeton University, Princeton, New Jersey, USA

Abstract Middle Carboniferous carbonates in the western U.S. have undergone Pleistocene Bahamas-style meteoric diagenesis that may be associated with expanding late Paleozoic ice sheets. Fourteen stratigraphic sections from carbonate platforms illustrate the regional distribution and variable intensity of physical and chemical diagenesis just below the Middle Carboniferous unconformity. These sections contain top-negative carbon isotope excursions that terminate in regional exposure surfaces that are associated with some combination of karst towers, desiccation cracks, fabric destructive recrystallization, or extensive root systems. The timing of the diagenesis is synchronous with similarly scaled top-negative carbon isotope excursions observed by others in England, Kazakhstan, and China. The mass flux of negative carbon required to generate similar isotopic profiles across the areal extent of Middle Carboniferous platform carbonates is a significant component of the global carbon cycle. We present a simple carbon box model to illustrate that the $\delta^{13}\text{C}$ of dissolved inorganic carbon in the ocean could be elevated by $\sim 1.4\text{\textperthousand}$ as isotopically light carbon from the weathering of terrestrial organic matter reacts with exposed platforms before reaching the ocean and atmosphere. These results represent an improvement on global biogeochemical models that have struggled to provide a congruent solution to the high $\delta^{13}\text{C}$ of the late Paleozoic icehouse.

1. Introduction

Ancient sediments from the late Paleozoic Era record climate change from a time period with tectonic, evolutionary, and oceanic-atmospheric boundary conditions vastly different than the Cenozoic. This geologic history represents an important opportunity to investigate the forcings and feedbacks of the climate system that cannot be gleaned from more recent archives. The ubiquitous diagenetic alteration of carbonates underlying a complex unconformable surface in the western U.S. that spans the Middle Carboniferous is presented here to constrain glacioeustatic change and to explore the potential impact that globally extensive meteoric diagenesis may have on the $\delta^{13}\text{C}$ of the ocean.

Extensive land ice during the late Paleozoic led to striated pavements, diamictites, dropstones, and glacial deformation structures across Gondwana [Fielding *et al.*, 2008]. Glacially derived sediments in Brazil, Bolivia, and Peru contain pollen and other microfossils from the latest Devonian [Caputo *et al.*, 2008; Isaacson *et al.*, 2008], suggesting possible Gondwanan ice sheets 360 million years ago. These South American ice sheets are thought to be followed by a 30–40 million year ice-free interval during the Tournaisian (358.9–346.7 Ma) and early Visean (346.7–330.9 Ma) [Isbell *et al.*, 2003]. By the start of the Serpukhovian (330.9–323.2 Ma), there is strong evidence of glaciation in both South America and Australia. Furthermore, detailed stratigraphic analysis of carbonate sections from the tropics indicate major facies distribution changes starting around this interval and persisting well into the Pennsylvanian [Bishop *et al.*, 2009, 2010; Fielding and Frank, 2015].

The early near-field glacial history could be explained by either large Gondwana-spanning ice sheets or smaller ice sheets that were growing and shrinking in various locations [Isbell *et al.*, 2003]. The oldest radiometric constraints on late Paleozoic glaciation are 60 million years younger than the end Devonian glacial sediments in South America [Stollhofen *et al.*, 2008; Cagliari *et al.*, 2014], and the inconsistencies in the early glacial records could reflect the difficulties of determining the depositional age of glacial sediments from biostratigraphy. Dry coastal climates from icehouse intervals are known to contaminate glaciers and glacial sediments with specious, old microfossils that weather out of exposed coastlines [Hoffman and Maloof, 2003; Kellogg and Kellogg, 1996]. Additionally, glaciers may erode and rework underlying stratigraphy before

filling a basin with new sediments, and the resulting stratigraphic limits on glacial processes will be too old. Combining the observations from glacial sediments with far-field, tropical marine sediments is a necessary tool for discovering the climate forcings that underpin both records. The importance of considering both records is demonstrated by studies from the Pleistocene, where resolving Northern Hemisphere glaciation required a synthesis of the discontinuous near-field glacial records and the more continuous deep-sea records [Imbrie and Imbrie, 1986; Emiliani, 1995].

The sedimentary record of Antarctic glaciation during the early Oligocene provides specific predictions for the response of platform carbonates during icehouse initiation. Carbonates on passive margins experienced 15–80 m of apparent sea level fall and largely were replaced by prograding deltas [Miller et al., 2005]. In response to ice growth and cooling, oceanic $\delta^{18}\text{O}$ shifted 1–1.5‰ higher, and an increase in ocean fertility [Baldauf, 1992] and major drop in the calcium carbonate compensation depth [Van Andel et al., 1975] may have led to 1–2 Myr of oceanic $\delta^{13}\text{C}$ enrichment by 1‰ [Zachos et al., 2001]. In the Early Carboniferous, carbon and oxygen isotopic shifts in platform carbonates mimic the observations from the Oligocene [Saltzman, 2002]. If analogous, this isotopic record suggests a Tournaisian initiation of the late Paleozoic ice age. However, the timing of this excursion overlaps with the 30–40 million year ice-free interval following the end Devonian glacial sediments from South America, indicating that the Gondwanan sedimentary record from the mid-Tournaisian is incomplete or that the $\delta^{13}\text{C}$ enrichment is not related to glaciation.

If the late Paleozoic icehouse began in the Early Carboniferous, then the globally extensive paleotropical sedimentary hiatus in the Middle Carboniferous may be evidence of land ice expansion. During the expansion of Northern Hemisphere glaciation during Plio-Pleistocene (~3 Ma), global sea level experienced an additional drop of 50 m [Miller et al., 2005], and the new lower-latitude ice albedo dynamics led to unstable ice sheets that varied periodically with orbitally driven solar insolation changes [Huybers, 2006]. The Bahama bank was exposed during the Plio-Pleistocene transition and after subsiding was subsequently flooded during each glacial-interglacial cycle. During exposure, meteoric fluids carrying isotopically light carbon and oxygen from the overlying soil system reacted with the calcium carbonate of the platform below [Swart and Eberli, 2005]. If the Middle Carboniferous hiatus is comparable to ice expansion in the Cenozoic, then the diagenetic reactions observed in the Bahama bank might be expected in carbonates below the stratigraphic horizon marking the expansion of late Paleozoic ice sheets.

1.1. Middle Carboniferous Hiatus

Shelf sediments on all major continents contain a significant hiatus during the Serpukhovian, and many carbonate sequences are replaced by siliciclastics prior to this hiatus [Saunders and Ramsbottom, 1986]. In the most complete sections, hiatus begins near the end of the Visean and deposition resumes in the Serpukhovian or Bashkirian (322.8–314.6 Ma). Deep basins lack a long-lived sedimentary hiatus (Cantabrian Mountains, Spain [Sanz López et al., 2006; Nemyrovska et al., 2011]) and can consist of repeating deep to shallow sedimentary cycles (Donets Basin, Ukraine [Eros et al., 2012]). The global correspondence of hiatus in shelf sediments and the continuous nature of deep water sections is consistent with a drop in sea level near the start of the Serpukhovian, and the deeper section cycles could indicate variable sea level during this interval. In North America, this interval famously is known as the Mississippian-Pennsylvanian boundary, and some regions of the shelf sediments in the western U.S. contain only 2–4 Ma of hiatus.

The Middle Carboniferous unconformity in the western U.S. caps extensive Tournaisian and Visean stable crinoidal and coralline carbonate banks known as the Madison Limestone in the north, the Leadville and Redwall limestones in the southeast, the Monte Cristo Group limestones in the southwest, and the Lake Valley Formation of southern New Mexico (Figure 1). The end Visean and early Serpukhovian is always missing in the unconformity, and hiatus in many sections spans a much wider range of time both above and below this interval (Figure 2). The unconformity is expressed as limestone karst towers and solution collapse breccia pits (Figure 4d) in Colorado, red terra rossa (Figure 4e), collapse breccia, dolomitization, and caves in Wyoming, and pervasively recrystallized carbonates capped in Stigmarian roots (Figure 4b), soils, sand-filled pits, and dissolution-collapse breccias (Figure 4a) in southern Nevada [Bishop et al., 2009].

These large-scale karst features indicate the importance of erosional processes inland and north of the Nevada sections, which could explain the wide range of ages for the immediately underlying strata. Post hiatus deposition across the region would be controlled by local subsidence, leading to variable ages in overlying sediments as well. All of these observations are consistent with sea level fall, exposure, and



Figure 1. Regional map of the western U.S. during the Mississippian subperiod. Blank regions represent highlands or regions with no Mississippian sediment preservation, and block texture represents marine carbonate deposition. Stratigraphic Sections studied are highlighted and color coded in correspondence with Figure 2. Diagonal lines are paleolatitude [Domeier et al., 2012].

porated by meteoric fluids moving through the overlying soil and vadose zone during exposure [Gross, 1964; Lohmann, 1988]. Carbonate minerals are unstable in the CO₂ charged meteoric fluids, leading to the dissolution and reprecipitation of the platform minerals [Budd, 1988]. The depth of this diagenetic freshwater lens is controlled by the distance from the coast, the local recharge rate, and the hydraulic conductivity of the carbonate rocks. As the underlying salt water is pushed down, the freshwater lens can extend well below mean sea level [Vacher et al., 1990].

While diagenetically altered carbonate platforms and karst terrains in the modern world represent a small fraction of sedimentary basins, the Early Carboniferous may have had the highest areal extent of neritic carbonates in Phanerozoic Earth history [Ronov, 1982; Walker et al., 2002; Peters, 2008]. These massive carbonates are coincident with the longest icehouse interval in the Paleozoic, where glacioeustatic change provided the opportunity for extensive meteoric diagenesis. The Middle Carboniferous unconformity may represent an initiation or major expansion of late Paleozoic glaciation, and the stratigraphy of this interval records the duration, lateral extent, and degree of diagenetic alteration of shallow carbonates. These observations, when coupled to carbon box modeling, provide a means to explore the impact of meteoric diagenesis on the δ¹³C of the late Paleozoic ocean and atmosphere.

2. Carbon Box Model

The mass flux of light carbon removed from the ocean and atmosphere and stored in altered carbonate rocks may have led to carbon isotopic enrichment of the ocean. A small modification to the carbon box model of Kump and Arthur [1999] can be used to evaluate the impact that such a process would have on the long-term evolution of ocean δ¹³C (Figure 3). The effect is analogous to that proposed for an authigenic carbonate sink [Schrag et al., 2013], though in this case, the respiration organic carbon is derived from the terrestrial biosphere, and the forcing is linked to glacioeustasy. The long-term isotope mass balance of the

erosion of the western U.S. carbonate shelf during the end Visean and may indicate expansion of land ice during the end Visean and Serpukhovian.

Evidence for exposure and sea level fall is expressed in the physical and chemical stratigraphy of western U.S. carbonates. In some areas, the regional unconformity is associated with at least 90 m of meteoric diagenesis, and a global trigger for this large-scale meteoric diagenesis is required to explain the presence of similarly scaled top-negative carbon isotope excursions in contemporaneous platform carbonates in the UK [Campion and Maloof, 2015], Kazakhstan [Ronchi et al., 2010], and China [Zhao and Zheng, 2014]. Furthermore, the presence of +2‰ δ¹³C in continuous deep water carbonates of northern Spain that span this interval [Buggisch et al., 2008] is evidence that the altered shelf sediments elsewhere are not recording the global dissolved inorganic carbon (DIC) of the ocean.

Isotopically light carbon in these shelf sediments is instead sourced, in part, from remineralized organic matter incor-

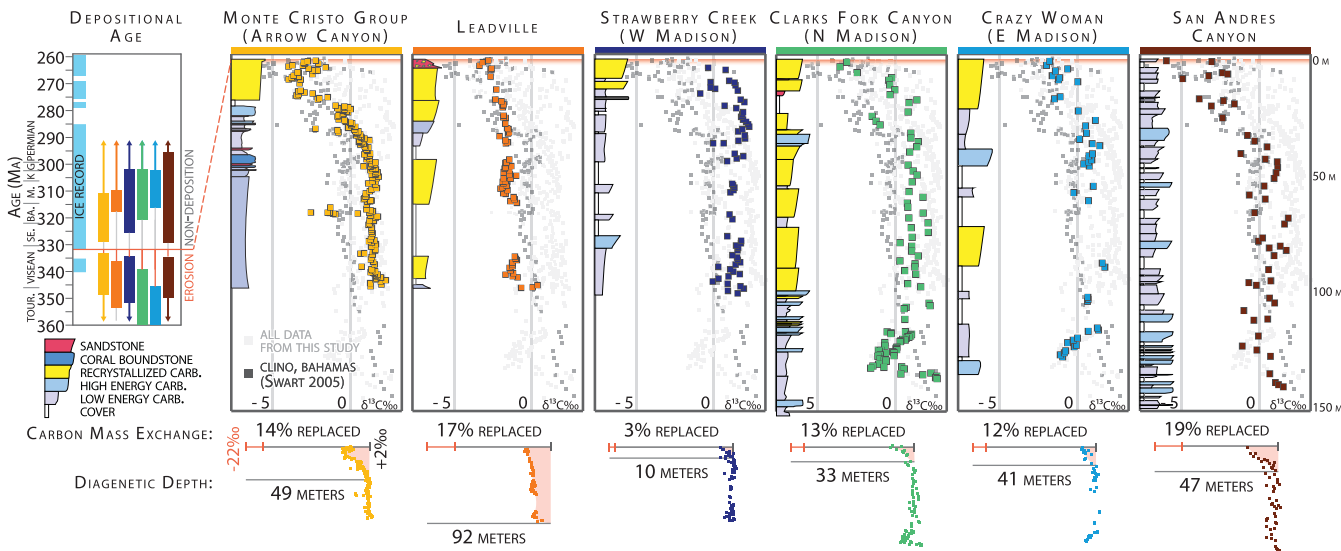


Figure 2. Carbon isotopes, depositional ages, and diagenetic reaction calculations for six stratigraphic sections from the Upper Mississippian (see Figure 1 for a map of section locations). Colored squares correspond to adjacent stratigraphy, while light gray squares indicate the data from all six sections. Dark gray small squares represent the upper 150 m of $\delta^{13}\text{C}$ from Clino core in the Bahamas which spans ~3 Ma [Swart and Eberli, 2005]. The diagenetic process is related to fluid flow from the upper exposure surface, and sections and data are hung by stratigraphic thickness from the exposure surface at 0 m. The light blue bar adjacent to the age timeline represents the ice record from the glacial sedimentary compilation in Montañez and Poulsen [2013]. Thick colored bars represent the biostratigraphic age of fossils contained in the rocks below and above the unconformity. Minimum mass exchange (pink area) calculations based on the percentage of soil carbon (−22‰) that would have to replace marine sourced (2‰) carbonate carbon to create the observed profile. The stratigraphic information has been simplified in this plot with high energy carbonates corresponding roughly to packstones and grainstones and low energy carbonates corresponding to micrites and wackestones. Recrystallized carbonates represent facies that have experienced significant coarse fabric-destructive recrystallization.

ocean and atmosphere is controlled by the carbon entering the system through weathering (F_w) and volcanism (F_{volc}) and the carbon leaving the system through carbonate ($F_{b,carb}$) and organic carbon ($F_{b,org}$) sedimentation:

$$\frac{dM\delta}{dt} = F_w \delta_w + F_{volc} \delta_{volc} - F_{b,carb} \delta_{carb} - F_{b,org} (\delta_{carb} + \Delta_B) \quad (1)$$

The weathering term ($F_w \delta_w$) is a combination of carbonate weathering ($F_{w,carb}$), and the weathering of organic matter in sediments ($F_{w,org}$). In times of low sea level, isotope exchange reactions during meteoric diagenesis (F_R) exchange low $\delta^{13}\text{C}$ terrestrial carbon with carbonate carbon, resulting in less isotopically light carbon ($F_{w,plat}$) entering the ocean and atmosphere. The dissolution of platforms (F_D) is allowed to exceed this reaction flux (F_R) to explore the model sensitivity to increased carbonate weathering during lowstands.

$$F_w \delta_w = F_{w,carb} \delta_{w,carb} + (F_{w,org} - F_R) \delta_{w,org} + F_D \delta_{w,plat} \quad (2)$$

Mass in the system is conserved by allowing the carbonate burial term to incorporate excess dissolved carbonate from platforms (F_D).

$$F_{b,carb} \delta_{carb} = (F_{b,carb} - F_R + F_D) \delta_{carb} \quad (3)$$

In order to quantify the reaction flux term in this model (F_R), limits must be placed on the extent, depth, and duration of meteoric diagenesis in the Middle Carboniferous.

3. Stratigraphy

Fourteen stratigraphic sections across the Middle Carboniferous unconformity in the western U.S. (Figure 1) were studied to document patterns of regional physical and chemical exposure features. To assess the ~10 km scale variability in diagenetic intensity, seven of these sections are located within a 14 km study area in the Arrow Canyon region of southern Nevada (Figure 7). Sediments were classified bed by bed into

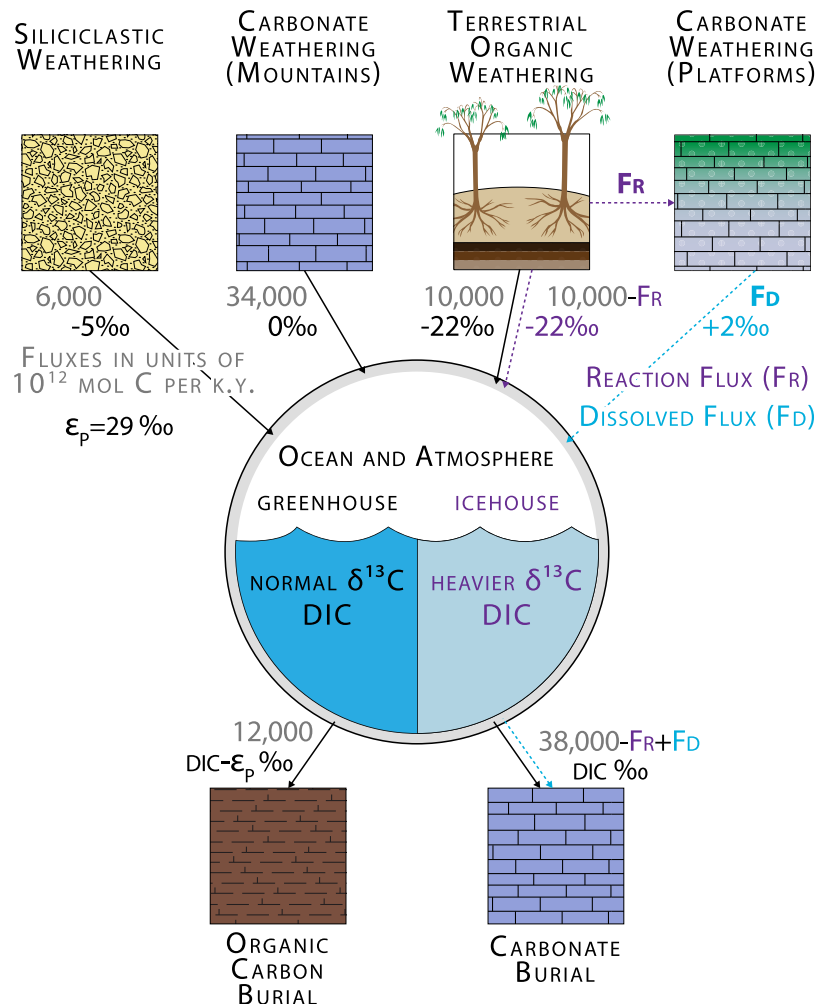


Figure 3. Carbon box model after Kump and Arthur [1999] (solid flux arrows). During glacial lowstand, remineralized soil-derived organic matter reacts with exposed carbonate platforms before entering the ocean and atmosphere (dashed flux arrows). This removal of light carbon from the ocean and atmosphere system leads to an enrichment in the $\delta^{13}\text{C}$ of the ocean DIC pool.

six lithofacies based on fossils, environmentally sensitive sedimentary structures, and the Dunham classification scheme for carbonates [Dunham, 1962]. From these sections, 1579 samples were collected at a half meter resolution and analyzed for $\delta^{13}\text{C}$ and $\delta^{18}\text{O}$ analysis. The hand samples were slabbed and polished to drill out carbonate powders for isotopic analysis. When possible, grains and shells were avoided and micrite was selectively sampled. Samples were hand polished and photographed, and individual textures, clasts, and shells were microdrilled to resolve millimeter-scale isotopic variations (Figures 5 and 6). All carbonate powders were heated to 110°C to remove water. Samples were then placed in individual borosilicate reaction vials and reacted at 72°C with five drops of H₃PO₄ before the CO₂ analyte was sent to the IRMS. Measured precision is $\pm 0.1\%$ for carbon and $\pm 0.2\%$ for oxygen. The samples were analyzed with either a Thermo DeltaPlus continuous flow IRMS or a Sercon IRMS coupled with a GasBench II sampling device. $\delta^{18}\text{O}$ and $\delta^{13}\text{C}$ data are reported in the standard delta notation relative to the Vienna Pee Dee Belemnite (VPBD) standard.

3.1. Monte Cristo Group, Nevada

The upper 50 m of the late Visean and early Serpukhovian carbonate shelf in southern Nevada hosts a gradual top-negative carbon isotope excursion [Bishop et al., 2009; Saltzman, 2005] that ranges from +2‰ at the bottom to -5‰ $\delta^{13}\text{C}$ at the exposure surface. Stable, thick bedded crinoidal wackestones and packstones of the Yellowpine Formation are capped in a 10–15 m thick *Lithostrotionella* coralline boundstone



Figure 4. Photographs of sedimentary features diagnostic of the Middle Carboniferous unconformity in the western U.S. (a) The contact between the Battleship Wash Formation carbonates and the dissolution-collapse breccia cap at the unconformity. The hand sample in Figure 5 was collected from within this breccia. (b) Stigmarian root impression at the hiatus contact in Arrow Canyon. (c) Photograph of the laterally continuous layer of black microcrystalline silica whose interior zonations are reminiscent of root. This layer is used as one of the stratigraphical tie points in Figure 7. (d) Dissolution-collapse breccia at the unconformable contact between the gray Visean Leadville Limestone and the overlying red Bashkirian Molas Shale, Little Molas Lake, CO. (e) Terra rossa surface diagnostic of hiatus surface of the platform carbonates exposed in the Salt River Range, WY (Strawberry Creek). Hammer head is 17.5 cm, pencil is 14.5 cm, marker is 14 cm, and coin diameter is 1.8 cm.

that can be traced for at least 14 km. Abundant low energy fenestral mudstones and articulated brachiopod-filled wackestones make up the next 10–15 m of section. Two parallel beds, separated by less than a meter of coarsely recrystallized carbonate, contain dense, branching networks of black microcrystalline silica whose interior zonations are reminiscent of root interiors (Figure 4c). These silicified root layers and the top of the *Lithostrotionella* coral beds were used as tie points for seven stratigraphic sections measured in the Arrow Canyon range and Meadows Mountains (Figure 7). Above the silicified roots, the carbonate is mostly coarse grainstone and packstone where it has not been completely recrystallized. In addition to macro-scale, outcrop-based identification of recrystallization, Bishop et al. [2009] found three sets of calcite cements that correspond to vadose zone, meteoric, and compaction lithification processes in thin sections from this upper interval of the Battleship Wash Formation. Sand-filled pits and abundant meter-sized stigmarian root casts (Figure 4b) mark the unconformity with the overlying Indian Springs Formation, which consists of 50–60 m of siliciclastics, soils, and thin diagenetically altered skeletal packstone carbonate beds. Biostratigraphy (compiled in

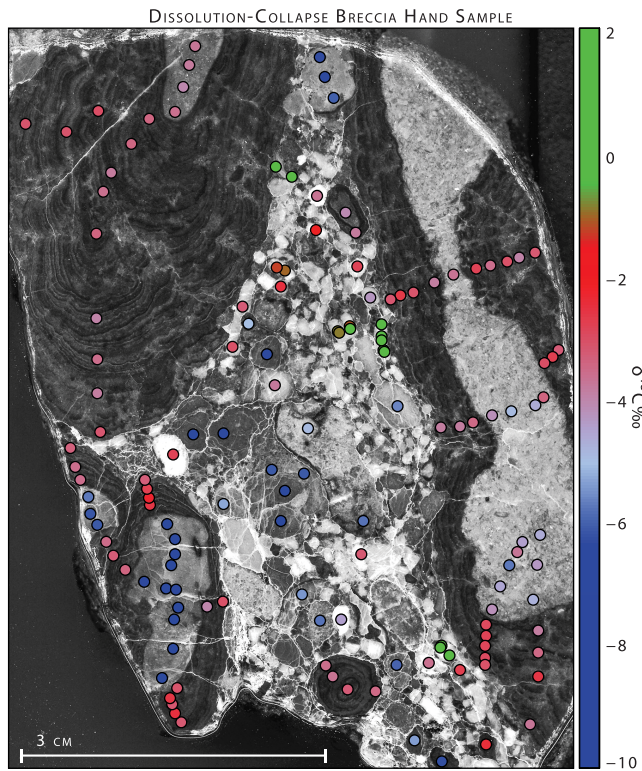


Figure 5. Hand sample of dissolution-collapse breccia from the top of the Battleship Wash Formation collected roughly 8 km north of Arrow Canyon, NV. Circles correspond to microdrilled $\delta^{13}\text{C}$ spot measurements, and the color scale indicates the isotopic value of that drill spot. Green data correspond to nonsparry brachiopods and crinoids. Large clasts are brecciated carbonate from the top of the Battleship Wash platform that have been coated by laminated black carbonate in a phytokarst environment. Uncoated shells, mud chips, and cements fill the interstitial space between large clasts.

and 7) and match global estimates for Visean seawater (Figure 12). Around 50 m below the unconformity, the carbon isotopes start to gradually decrease upward to minimum values of $-4.5\text{\textperthousand}$ just below the hiatus. The depth and intensity of carbon isotopic alteration generally increases from South to North in the Monte Cristo Group study area, and is not consistent from section to section. In Figure 7, interpolation of carbon isotopic data between sections highlights the diagenetic pattern of the carbonate shelf. Some microdrilled shells from breccia hand samples (Figure 5) at the top of this sequence just below the hiatus are isotopically similar to the values at the bottom of the excursion ($+2\text{\textperthousand} \delta^{13}\text{C}$). The range of isotopic compositions for different features in the hand samples is larger than the outcrop variability (Figure 6). The large coated clasts have the lowest carbon isotopes (-5 to $-8\text{\textperthousand} \delta^{13}\text{C}$), the black laminated coatings are slightly higher (-2.5 to $-5\text{\textperthousand} \delta^{13}\text{C}$), and the shells are highly variable with values from $-4.5\text{\textperthousand}$ to $+2.1\text{\textperthousand} \delta^{13}\text{C}$. Only the shells exhibit oxygen isotopes higher than $-4\text{\textperthousand}$ and carbon isotopes higher than $-3\text{\textperthousand}$ (Figure 5), and shells that have coarsely crystalline (sparry) textures have lower carbon isotopes than shells that have nearer to original biogenic textures.

3.2. Leadville Limestone, Colorado

The U956 and D751 cores through the Leadville Formation consist of interbedded limestone and dolomite wackestones where the dominant allochems are large articulated crinoids. The unconformity at the top of the formation is an irregular contact with limestone dissolution-collapse breccia containing interstitial red shale of the overlying Molas Formation. Around Little Molas Lake, Colorado, limestone karst towers and solution collapse breccia pits at this contact are well exposed. Biostratigraphy of the Leadville limestone indicates middle Tournaisian to middle Visean age [Fouret, 1996]. The overlying Molas Shale is late Bashkirian, so the interval of time missing at the unconformity is roughly 20 million years (Figure 2). Carbon isotopes of the carbonates

Bishop et al. [2009]) indicates that this interval of hiatus corresponds to a single missing conodont zone that may represent up to 4 Ma (Figure 2) when the biostratigraphic units are correlated with global, radiometrically constrained biostratigraphic boundaries [Davydov et al., 2012]. Despite poor exposure of the unconformity surface, it appears that the carbonates of the Battleship Wash Formation are immediately overlain by a thin, fine-grained, and distinctly rippled red-brown sandstone. This sandstone is found over the entire 14 km study area, and is illustrated by the red circle icon in Figure 7. In the north, this rippled sandstone lies directly above carbonate breccia-filled channels and pits (Figure 4a) of a phytokarst [Folk et al., 1973] terrain that corresponds to erosion of the upper Battleship Wash carbonates. The carbonate breccias contain clasts of limestone from the upper part of the Battleship Wash Formation, and many clasts are coated by black, submillimeter laminated carbonate up to 5 cm thick. However, within the same breccia pits, some smaller clasts and intact shells are completely uncoated (Figure 5).

Carbon isotopes at the bottom of the sections have low variance (Figures 2

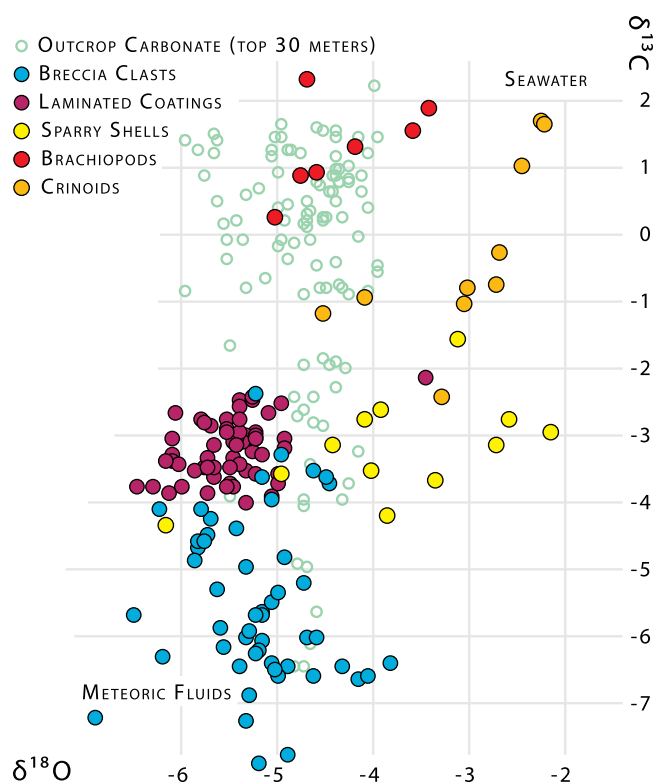


Figure 6. Carbon and oxygen isotope cross plot illustrating the high seawater $\delta^{13}\text{C}$ values recorded in pristine shells, and the low meteoric values recorded in clasts from the breccia hand samples (Figure 5) and in the 30 m of carbonates directly below the unconformity in Arrow Canyon.

north to south (Figure 1). The western most section, measured along Strawberry Creek in the Salt River Range, is 93 m of mostly wackestone. The upper 15 m are increasingly brecciated and recrystallized, and the unconformable top is a 1 m thick red, irregular, sand-filled pedogenic layer. The $\delta^{13}\text{C}$ of the section is consistently between +2 and +3‰ with a slight decrease in the upper 10 m to values as low as 0‰. At Clark's Fork Canyon in northern Wyoming, 230 m of Madison limestone outcrop along the northern canyon wall. The lower 120 m are made up of stacked carbonate parasequences that contain the mid-Tournaisian double-peaked positive isotope excursion (Figure 12) first documented in *Saltzman* [2002] (up to +7.3‰ $\delta^{13}\text{C}$). The textures and facies of the upper 110 m have been completely erased by brecciation and recrystallization. The carbon isotopes in this interval are between +1 and +2‰, until the upper 16 m where there is a top-negative carbon isotope excursion that goes from +2 to -4‰ $\delta^{13}\text{C}$. The unconformity at the top is irregular with several meters of pitted relief, including a 5 m deep sand-filled paleo-sinkhole (described in *Sando* [1988]). The eastern extreme of the Madison Shelf, at Crazy Woman Canyon, is comprised of 130 m of dolomite that terminates in brecciated carbonate, followed by red sandstones that are 15–20 million years younger [*Sando*, 1988]. Meters 40–60 contain the double-peaked positive carbon isotope excursion of the Tournaisian (Figure 12), followed by 35 m of +2‰ $\delta^{13}\text{C}$. The remaining 20 m contain a top-negative $\delta^{13}\text{C}$ excursion that goes from +2 to -2‰.

3.4. San Andres Canyon, New Mexico

Dark gray limestone mudstone to coarse-grained, cherty, crinoidal grainstone and packstone of the Lake Valley and Rancheria Formations in the San Andres mountains are unconformably overlain by 10–15 m of black shale that contains conodonts from the end of the Visean. Exposure features such as mud cracks and root casts are present in the upper 60 m of the underlying carbonates. Some medium to thick grainstone beds have silicified tops, but unlike the other sections described above, there is no pervasive, fabric destructive recrystallization apparent at the outcrop scale. However, three generations of meteoric, marine, and mixing zone cements in thin sections from the carbonate beds below the unconformity are attributed to

below the unconformity in both U956 and D571 (30 km apart) are low (<0‰) for nearly 100 m and get increasingly lower toward the upper contact with the dissolution-collapse breccia and Molas Formation.

3.3. Madison Shelf, Wyoming

A regional unconformity at the top of the Madison shelf is present throughout Wyoming. The western margin of the shelf is more continuous, and the unconformity is well constrained by conodont biostratigraphy to be end Visean [*Sando*, 1988; *Batt et al.*, 2007]. The stratigraphic hiatus represented by the unconformity increases to the east due to a combination of both older underlying and younger overlying sediments (Figure 2). This pattern could result from a time-transgressive nondepositional surface and increasing erosion inland (eastward) [*Sando*, 1988].

Sections from Strawberry Creek, Clark's Fork Canyon, and Crazy Woman Creek span a range of 350 km east to west and 200 km

reactions during fluid flow associated with sea level draw down [Meyers, 1985; Frank *et al.*, 1995]. Carbon isotopes in the lower 100 m of this formation are highly variable with values ranging from $-2\text{\textperthousand}$ to 2\textperthousand . Carbon isotopes get progressively more negative over the 46 m below the unconformity, with minimum values of $-5\text{\textperthousand}$ at the top.

4. Discussion

4.1. Primary Versus Diagenetic $\delta^{13}\text{C}$

When changes in $\delta^{13}\text{C}$ are observed in time-correlative sections across hundreds of kilometers and in different basins, it often is assumed that the carbonates are recording secular changes in the isotopic value of dissolved inorganic carbon in the global ocean. However, carbon isotopic variations in carbonate can be generated by diagenetic reactions associated with glacioeustasy [Swart and Eberli, 2005]. Each of the late Paleozoic sections described in this paper has top-negative carbonate $\delta^{13}\text{C}$ excursions terminating in subaerial exposure surfaces (Figure 2). The isotopic variation of $8\text{--}9\text{\textperthousand}$ in $\delta^{13}\text{C}$ and 20–100 m scale is comparable to the variation and scale observed in the Pleistocene of the Bahamas [Swart and Eberli, 2005] (Figure 2). Despite these similarities, secular changes in DIC cannot immediately be ruled out as environmental change and carbon isotopic excursions often are coincident. Diagenetically screened brachiopods from within the isotopic excursion in Arrow Canyon are isotopically much heavier than the micritic carbonate from the same stratigraphic intervals [Bishop *et al.*, 2009; Brand *et al.*, 2012]. The presence of shells at the top of the excursion (Figures 5 and 6) that have $\delta^{13}\text{C}$ values that match the carbonate values below the excursion ($+2\text{\textperthousand}$) is further indication that seawater DIC was not changing much below the unconformity. Additionally, these isotopically heavy shells have the same range of isotopic values that were measured by Buggisch *et al.* [2011] in time correlative deep pelagic carbonates in Spain (Figure 12). The magnitude of isotopic variability observed between micrite and select shells throughout the isotopic excursion is inconsistent with the top-negative excursion recording primary changes in global ocean DIC. Instead, the light isotopes can be explained by partial equilibration with diagenetic meteoric fluids, where locally decreased permeability around select shells, as well as their interior less permeable microstructure, allowed them to remain closed to the altering fluids.

4.2. Timing of Diagenesis

Sedimentary hiatus is a combination of erosion and nondeposition, and meteoric diagenesis below the unconformity could correspond to a single long diagenetic event or any number of short events spanning the interval of time missing. Diagenesis caused by glacioeustasy should be roughly synchronous around the world, and meteoric diagenesis should be recorded where that glacioeustasy resulted in exposure and sedimentary hiatus. Due to erosion and nondeposition during the hiatus, there is no unambiguous test for diagenetic synchronicity among the sections. However, glacioeustasy should lead to hiatus that span some common interval of time, and the smallest single interval of hiatus provides the best estimate for the timing of this glacioeustatic change.

As the global stratotype section and point (GSSP) for the Mississippian-Pennsylvanian boundary [Lane, 1999], the Arrow Canyon section has some of the best biostratigraphy in the late Paleozoic. This section is almost continuous through this interval, but a conodont zone that represents 2–4 million years of the end Visean is missing between Battleship Wash carbonates and the overlying Indian Springs Formation (biostratigraphy compiled in Bishop *et al.* [2009]). This timing is consistent with the Lake Valley carbonates from New Mexico. The carbonates below the unconformity contain middle Visean conodonts, and the overlying Helms Shale contain conodonts from the end of the Visean and early Serpukhovian [Bachtel and Dorobek, 1998; Proske, 2013]. While spanning much larger time intervals, hiatus in Leadville and the Madison Shelf sections overlap with this late Visean window (Figure 2), so if the diagenetic excursions across the western U.S. are from a single late Visean episode, then erosion is responsible for older underlying sediments and variable nondeposition is responsible for younger overlying sediments. A glacioeustatic driver for meteoric diagenesis of the western U.S. carbonate shelf explains similarly scaled top-negative carbon isotopic excursions from platform carbonates in Kazakhstan [Ronchi *et al.*, 2010], China [Zhao and Zheng, 2014], and the UK [Campion and Maloof, 2015] at the end of the Visean and early Serpukhovian (Figure 12). This timing roughly corresponds to the turning on of near-field glacial sedimentation in Australia and South America [Montañez and Poulsen, 2013]. In addition, the ongoing formation of Pangea may have played a role in the

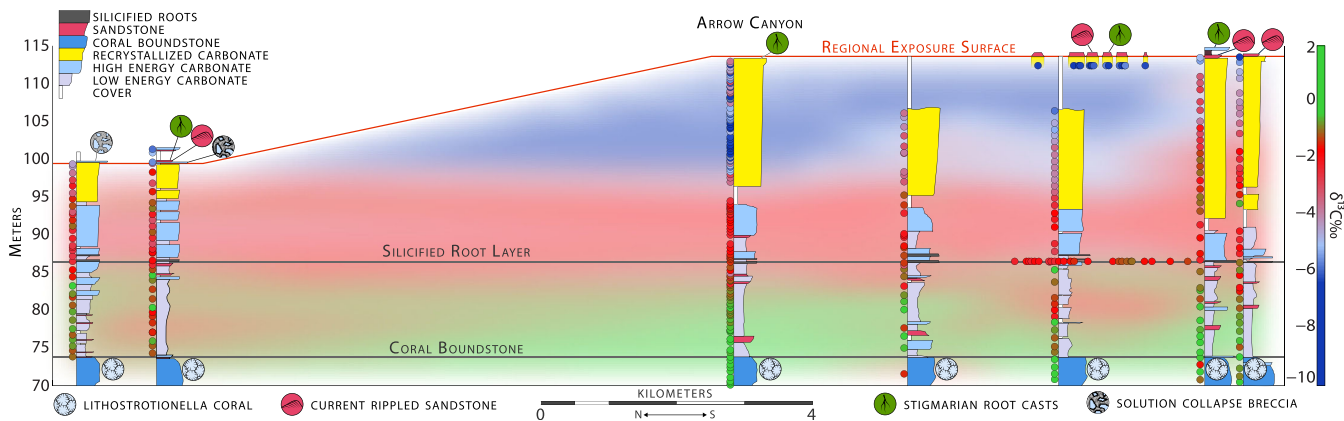


Figure 7. Lateral (North to South) transect of the Battleship Wash Formation of southern Nevada, centered on Arrow Canyon. Sections are tied together by two laterally continuous stratigraphic units that are easily identified and were traced on foot over the study interval (gray lines). The regional exposure surface is identified by a combination of roots (Figure 4b), recrystallized texture, blue-gray to brown coloration change, and a distinctive overlying current rippled fine sandstone. Circles correspond to isotopic measurements on carbonate from the adjacent stratigraphy, and the colored background is a smoothed two-dimensional linear interpolation of these isotopic data. Refer to caption of Figure 2 for facies description.

tectonic uplift of some of these carbonate platforms, perhaps resulting in meteoric diagenesis. Regardless of the mechanism behind the pervasive platform diagenesis, the presence of low $\delta^{13}\text{C}$ in carbonates around the world over a narrow span of time likely had an impact on the global carbon cycle.

4.3. Constraining the Magnitude and Rate of Sea Level Fall

At the < 10 km scale, the depth of meteoric diagenesis is controlled by local forcings, such as rainfall and rock permeability [Vacher et al., 1990]. Over larger length scales, the presence of diagenesis in many stratigraphic sections from the same exposure interval is evidence for regional changes in base level due to glacioeustasy or tectonics. When the same diagenesis is observed globally (Figure 12) at a time period when polar sedimentary basins are filled with glacially derived sediments [Fielding et al., 2008], then a glacioeustatic forcing for the diagenesis is probable. Ideally, the average depth of diagenesis across many stratigraphic sections would offer some insight into the scale of glacioeustatic fall. However, given the 10–100 m of variability in the depth of diagenesis at the regional (Figure 2) and kilometer (Figure 7) scale observed in the sections presented in this paper, the local forcings in each location appear to overshadow information about the magnitude of glacioeustatic change.

If the subsidence of a sedimentary basin can be constrained, base level change potentially is recorded in the duration of stratigraphic hiatus. The biostratigraphic time scale from Arrow Canyon places limits on the duration of exposure at the end of the Visean. When coupled to a subsidence model, these limits can be used to estimate the drop in global sea level and infer the corresponding change in land ice volume at this time. Carbonates of the western U.S. during the Devonian and Early Carboniferous were deposited on a broad forebulge associated with the Antler Orogeny [Dickinson, 2006]. Subsidence during the early and Middle Carboniferous in the Arrow Canyon region is slow and constant (Figure 8a), suggesting that a simple linear model for subsidence may provide some insight into the change in base level at the unconformity. Assuming that Indian Springs Formation was deposited at sea level, and deposition initiated as soon as the exposed carbonates subsided to the new mean sea level, then the difference between the accumulated thickness of sediments and the linear fit subsidence model should correspond to a change in sea level. If this assumption is incorrect and the deposition of the Indian Springs begins below sea level, then the sea level change calculated here is an underestimate. Most likely, the biostratigraphic age uncertainty outweighs this depositional height uncertainty. To simulate the uncertainties associated with the biostratigraphy, this calculation was performed 10,000 times allowing each biostratigraphic interval to vary with a normal distribution over individually assigned uncertainties. The estimated sea level drop required to explain the difference between accumulation and the subsidence model from these calculations is 29.8 ± 7.8 m (Figure 8b). In order to evaluate the sensitivity of this calculation to the assigned uncertainties, 40 new sets of 10,000 calculations were performed for 2σ errors at 0.1 Ma intervals between 0 and 4 Ma (Figure 8c). From the sensitivity test, it is clear that if biostratigraphic uncertainties are ± 4 Ma, then this calculation cannot resolve changes in sea level. However, if the biostratigraphy is accurate to 2σ between 0.5

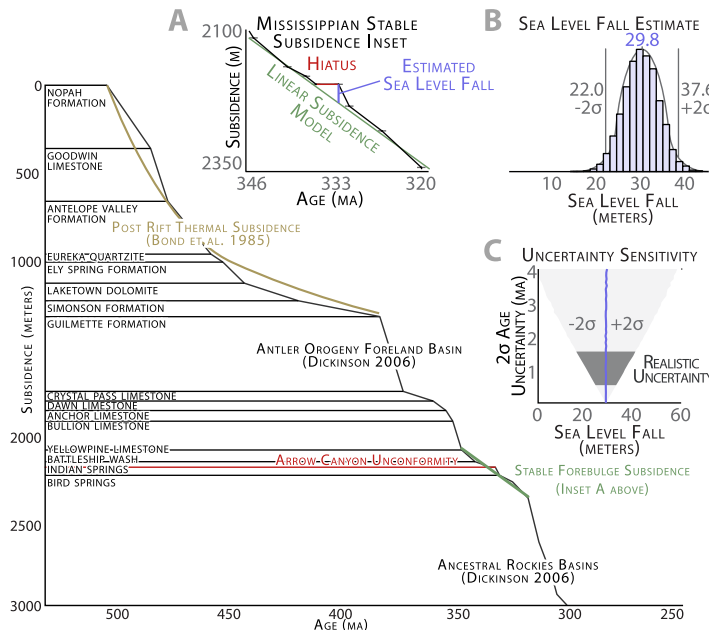


Figure 8. Cumulative stratigraphic thickness of sediments through time in the region of Arrow Canyon, beginning above with the Great Unconformity of the Cambrian. Cambrian and Ordovician accommodation space is dominated by postrifting thermal subsidence [Bond *et al.*, 1985]. Accommodation in the Antler Orogeny foreland basin through the Devonian and Carboniferous [Dickinson, 2006] lead to constant accumulation rates during the Middle Carboniferous. (a) Assuming linear subsidence during the Middle Carboniferous of Arrow Canyon, where biostratigraphy constrains the maximum length of hiatus to be 4 ± 1 Ma, sea level fall is calculated by the difference between post hiatus accumulation thickness and the modeled expected subsidence. (b) By including the biostratigraphic uncertainties for each boundary during this interval, sea level fall can be estimated to 30 ± 8 m. (c) The relationship between age uncertainty and the range of sea level fall estimates.

and 1.5 Ma, the sea level change estimate and calculated errors are robust for this simplified linear subsidence model.

The sea level change estimates of 30 ± 8 m are comparable to the glacioeustasy associated with the initiation of Northern Hemisphere glaciation [Miller *et al.*, 2005], suggesting that the analogy to the Plio-Pleistocene expansion of the Cenozoic icehouse may be relevant for the Middle Carboniferous. With almost no Northern Hemisphere continents at this time, all of the glacioeustasy would have been accommodated by expansion of the Southern Hemisphere Gondwanan ice sheets. Accounting for continental shelf isostatic effects that result from glacioeustasy [Hughes and Denton, 1981], an ice volume growth of $12.5\text{--}21.4 \times 10^6$ km 3 is required to account for these estimates of glacioeustasy. The upper end-member overlaps with the maximum ice volume estimated from the late Paleozoic glacial sedimentary record of $20 \pm 2 \times 10^6$ km 3 [Montañez and Poulsen, 2013], suggesting that ice volume in the Middle Carboniferous may have approached maximum ice volumes for the late Paleozoic icehouse or that the near-field records have underestimated global ice volume.

4.4. Carbon Cycle Budget

Meteoric diagenesis of subaerially exposed carbonate platforms in the Middle Carboniferous likely was a global phenomenon, and the total amount of light carbon exchanged with each sedimentary section is presented in Figure 2 (bottom). Reaction percentages are calculated by a simple two-component mixing of original $+2\text{\textperthousand}$ $\delta^{13}\text{C}$ and organically derived carbon ($-22\text{\textperthousand}$ $\delta^{13}\text{C}$). The reaction mass flux (F_R) is estimated by multiplying the reaction percentages by a volume of reacted carbonate (based on areal extent of platforms and depth of diagenesis) and dividing by the time scale of diagenesis. Figure 9a shows the temporal evolution of three model simulations with a constant reaction flux (F_R) and a range of platform dissolution fluxes (F_D) to simulate the sensitivity to potential increased weathering from newly exposed carbonates. Figure 9b depicts the results of 100,000 model simulations where carbonate platform area, platform dissolution, duration and depth of diagenesis, and reaction percentages all are allowed to vary. The duration of diagenesis is based on the duration of hiatus at Arrow Canyon and is input into the simulations as a normal distribution

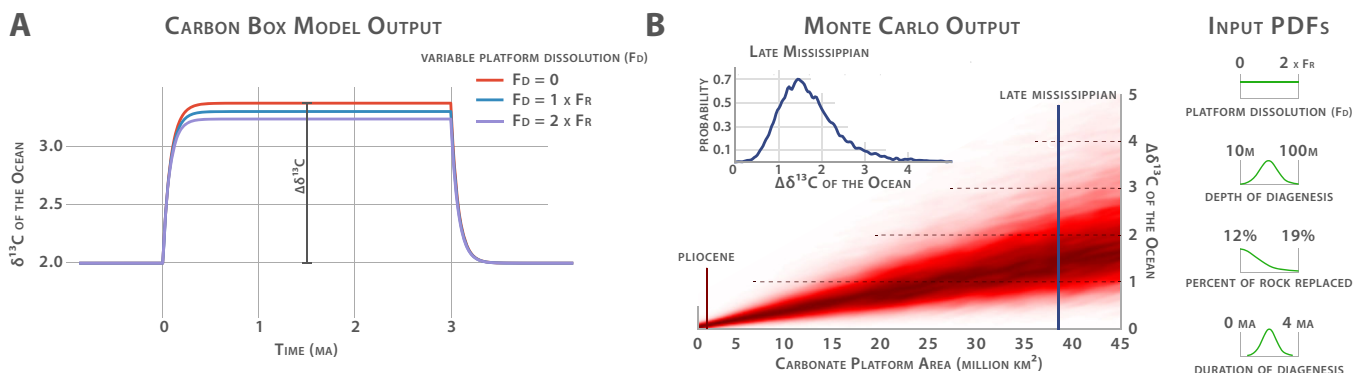


Figure 9. (a) Carbon box model simulation with a reaction flux (F_R) of 2700×10^{12} mol C per kyr with variable platform dissolution (F_D). (b) Two-dimensional histogram of 100,000 iterations of the carbon box model with variable carbonate platform area, platform dissolution, duration and depth of diagenesis, and reaction percentages. Each parameter was randomly drawn from the distributions illustrated on the right. The estimated probability density function corresponding to the model results for the diagenesis of Late Mississippian carbonate platforms is illustrated in blue (area from Walker *et al.* [2002]).

with a mean of 2 Ma and a standard deviation of 0.5 Ma. The distributions for the depth of diagenesis and reaction percentages are conservative estimates based on the geochemical data from each stratigraphic section plotted in the Figure 2 (bottom), and the platform dissolution flux is allowed to vary with a uniform distribution between 0 and 2 times the diagenetic reaction flux. Using a minimum estimate for Late Mississippian carbonate platform area of 39 million km² [Walker *et al.*, 2002], there is a 95% probability that the ocean DIC was 0.6–2.9‰ heavier due to meteoric diagenesis, with a maximum probability peak at +1.4‰. When the same model parameter distributions are applied to the much smaller carbonate platform areas of the Pliocene [Walker *et al.*, 2002], there is a 95% probability that the change in ocean DIC associated with meteoric diagenesis is less than 0.3‰.

4.5. Implications for Biogeochemical Models

Positive excursions in the carbonate $\delta^{13}\text{C}$ record commonly are interpreted as increases in the global fraction of organic carbon buried (relative to carbonate), and the burial of organic carbon decreases the oxygen removed from the ocean and atmosphere during remineralization, leading to an increase in oxygen concentrations through time [Berner, 2006]. While the coals of the Upper Carboniferous indicate significant organic carbon burial on land [Phillips and Peppers, 1984; Cleal and Thomas, 2005], the model presented above suggests that meteoric diagenesis also may contribute to the observed isotopic enrichment of oceanic DIC (Figure 12). This enrichment could be sustained if these reactions remain important throughout the late Paleozoic, perhaps primarily during intervals of high-amplitude glacioeustasy (Figure 10).

The high $\delta^{13}\text{C}$ of the ocean is a major component in Phanerozoic atmosphere oxygen models such as GEOCARBSULF [Berner, 2006]. This model determines atmospheric oxygen concentrations during the late Paleozoic as high as 30%, but concentrations much higher than 25% would result in strong negative feedbacks in the fire system that should result in the collapse of terrestrial plant ecosystems [Belcher *et al.*, 2010].

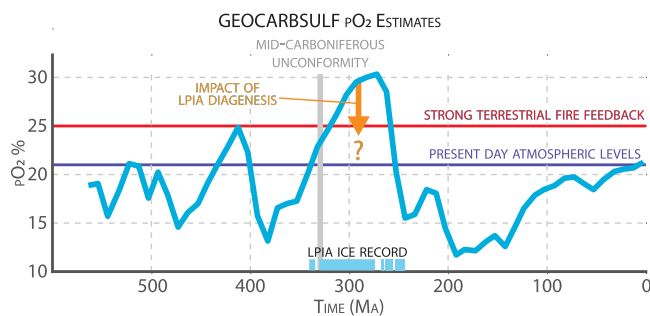


Figure 10. GEOCARBSULF pO_2 % estimates from Berner [2006]. Meteoric diagenetic reactions of exposed carbonates during the late Paleozoic glaciation would result in lower pO_2 estimates for this time interval.

While there is some evidence of increased fire during the Carboniferous [Scott and Glasspool, 2006; Glasspool and Scott, 2010], the presence of coal swamps and forests throughout the Pennsylvanian and Permian indicate that oxygen levels were probably not much higher than 25%. The COPSE biogeochemical model [Bergman *et al.*, 2004] uses a set of six biological and geological forcings (volcanic degassing, tectonic uplift, land plant colonization, land plant weathering enhancement, deep pelagic carbonate sink, and solar luminosity) to

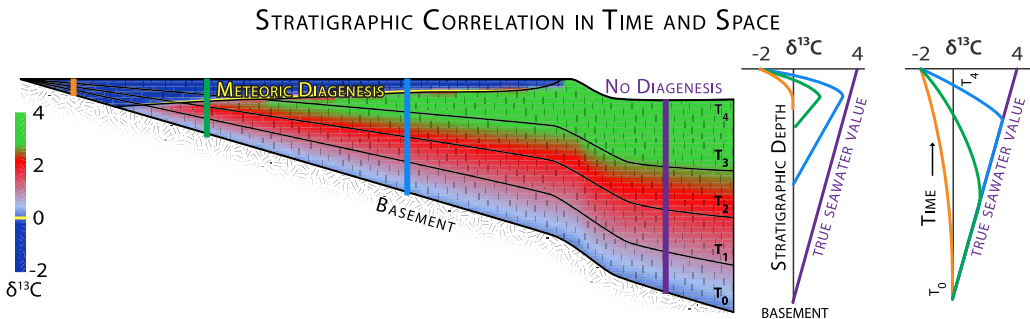


Figure 11. Synthetic basin illustrating how spatial diagenetic signals manifest in data sets based on depositional times. Timelines correlate sections of variable sedimentation rates. Similarly scaled diagenetic profiles cover longer intervals of stratigraphic time in sections with low sedimentation rates (orange) when compared to sections with higher sedimentation rates (blue). Diagrams on the right depict the relationship of each section when the isotopic values are plotted versus either (right) stratigraphic time (potentially derived from biostratigraphy or radiometric ages from interbedded ashes) or (left) stratigraphic depth.

estimate the pO_2 reservoir (and many others) through the Phanerozoic and provides more reasonable oxygen compositions during the Carboniferous ($\sim 25\%$). Rather than using the $\delta^{13}C$ record as an input, this model predicts $\delta^{13}C$, and comparison to the record provides a good test for the model. While generally the model predictions match the ancient record very well, it severely underestimates ($1\text{--}3\text{\textperthousand}$) the carbonate $\delta^{13}C$ record during the late Paleozoic Ice Age (Figure 12). High oxygen estimates from GEOCARBSULF and underestimated $\delta^{13}C$ of DIC from COPSE can be reconciled if the high $\delta^{13}C$ of late Paleozoic oceans (Figure 12) is in part caused by light carbon reacting with carbonate platforms during meteoric diagenesis (Figure 9).

4.6. A Global Perspective From Compiled Carboniferous $\delta^{13}C$

Figure 12 depicts 5225 compiled Carboniferous $\delta^{13}C$ data points from this study and published literature [Batt *et al.*, 2007; Buggisch *et al.*, 2011, 2008; Mii *et al.*, 1999; Saltzman, 2005; Ronchi *et al.*, 2010; Zhao and Zheng, 2014; Bruckschen *et al.*, 1999; Koch *et al.*, 2014] with all age boundaries remapped into a single up-to-date time scale [Davydov *et al.*, 2012]. Negative isotopic excursions associated with meteoric diagenesis introduce significant scatter in the carbon isotopic record. Meteoric diagenesis is expressed over length scales of zero to hundreds of meters, and a single diagenetic event will overprint very different stratigraphic ages in sections containing different accumulation rates. Figure 11 illustrates this concept with a computer generated synthetic basin where ocean DIC increases from 0 to 4\textperthousand over arbitrary time steps t_0 to t_4 . Thus, assuming that the diagenetic $\delta^{13}C$ of the rock corresponds to the depositional age of that rock will lead to spurious carbon isotope-based correlations in time (see Leadville in Figure 12).

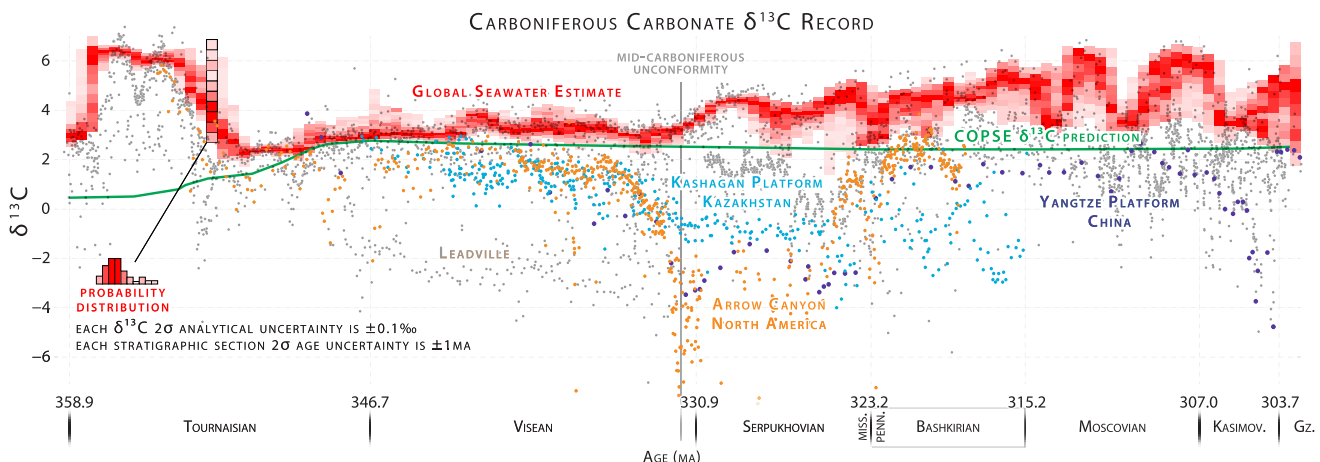


Figure 12. Estimated (red) $\delta^{13}C$ of DIC from data presented here and literature compilation. All data have been remapped into the age boundaries found in Davydov *et al.* [2012]. Monte Carlo weighted bootstrap resampling of the data with uncertainties is used to generate seawater $\delta^{13}C$ DIC estimates. Seawater estimates increase at the mid-Carboniferous unconformity and platform carbonates from three continents contain low carbon isotopic values throughout the Serpukhovian. Leadville carbonates are an example of diagenesis that spans stratigraphic intervals that do not match the timing of alteration (Figure 11).

With high enough sampling density, spurious low $\delta^{13}\text{C}$ data can be filtered out by placing more weight on high carbon isotopic values. Diagenetic fluids are unlikely to drive carbon isotopes to values higher than ocean water, so high carbon isotopic values from open marine settings provide the best estimate for global ocean DIC. These ideas can be applied to the vast record of published Carboniferous $\delta^{13}\text{C}$. Means were calculated by weighted bootstrap resampling of the data within 0.5 Ma bins across the data set. Two sets of weights were designed for the data set to recreate global seawater DIC estimates. One weighting gives all data points within 1‰ of the maximum in that bin a uniform weight, and the distance below this 1‰ window leads to exponentially less probability to be resampled. To remove differences in the chemostratigraphic sampling resolutions among data sets, the second set of weights are inversely proportional to the sample density in time– $\delta^{13}\text{C}$ space. Histograms of the weighted bootstrap means for each time bin are illustrated as red boxes, where color intensity represents probability. While this weighted bootstrap approach may overlook potential isotopic differences between ocean basins [Mii *et al.*, 1999], it serves to highlight the first-order differences between the Late Mississippian and Pennsylvanian oceans.

Platform sediments in North America, Kazakhstan, and China contain significantly lower $\delta^{13}\text{C}$ than global seawater estimates during the Middle and Late Carboniferous (Figure 12). Meteoric diagenesis is not limited to the end-Visean as presented in this study. Unstable ice sheets and the resulting glacial-interglacial cycles may be a mechanism for meteoric diagenesis throughout the late Paleozoic Ice Age. Small-scale (1–5 m) meteoric diagenesis has been documented in Upper Carboniferous sections from the western U.S. [Elrick and Scott, 2010; Dyer and Maloof, 2015]. Expanding on the model relationships illustrated above, a sustained meteoric diagenesis flux that begins at the end-Visean could explain some portion of the observed ~2‰ increase in global seawater DIC in the Upper Carboniferous (Figure 12).

4.7. Groundwater-Rock Reactions and Plant Evolution

The evolutionary developments of forest and soil ecosystems during the middle Devonian seem to mark a fundamental change in the way meteoric diagenesis is recorded in carbonates. Phases reacting with meteoric fluids at the top of a platform are in open exchange with atmospheric carbon, dissolved rock carbon, and remineralized terrestrial organic carbon. Further away from atmospheric and terrestrial carbon inputs (downward), the fluids are rock buffered. For meteoric diagenesis to lead to carbon isotopic excursions, the open system inputs must be isotopically distinct from the ocean and atmosphere system that the carbonates precipitated from.

During the Devonian, the increase of tree distribution and depth of root penetration resulted in a large increase in the thickness and areal extent of soils [Algeo and Scheckler, 1998], which are a source of isotopically distinct carbon to subsurface freshwater systems. Exposed platform carbonates from before the Devonian that contain many of the same karst-terrain features documented in the Middle Carboniferous are not associated with carbon isotopic excursions [Jones *et al.*, 2015], suggesting that the open system fluids of that time (Hirnantian) lacked significant isotopically distinct carbon. Older isotopically light carbonates from the Neoproterozoic have been interpreted to have derived their low $\delta^{13}\text{C}$ values from Earth's first terrestrial photosynthesizers [Knauth and Kennedy, 2009; Swart and Kennedy, 2012]. While these carbonates rest below glacial unconformities, they lack top-negative carbon isotopic excursions, and both platform chemostratigraphies and carbonate clasts from overlying diamictites indicate that the carbonate platforms acquired their $\delta^{13}\text{C}$ anomalies prior to glacial truncation [Halverson *et al.*, 2002; Rose *et al.*, 2012]. If Cryogenian carbonates like the Trezona Formation [Rose *et al.*, 2012] were altered during glacioeustatic drawdown, then the altering meteoric fluids were not carrying significant amounts of isotopically light carbon.

5. Conclusion

A long hypothesized period of land-ice expansion in the Middle Carboniferous is supported by the observations of globally synchronous meteoric diagenesis of carbonate platforms. This climate change corresponds to a 2‰ increase in the $\delta^{13}\text{C}$ of DIC and a shift from stable, monotonous shallow carbonate sediments that pervade the Visean to cyclic stacks of shallowing upward parasequences in the Serpukhovian and Bashkirian. Such a change in shelf sedimentation could reflect an increased glacioeustatic sedimentary forcing caused by large, unstable ice sheets that formed during the Middle Carboniferous unconformity.

The burial flux of organic carbon exerts a dominant control on atmospheric CO₂ and O₂ on long geologic time scales. The isotopic value of the dissolved inorganic carbon in the ocean is recorded in carbonates

through time, and secular changes in this value frequently are interpreted as changes in the burial flux of organic carbon. The isotopically light carbonate platforms from the Middle Carboniferous are inconsistent with this simple model, because remineralized, light, organic carbon has been removed from the ocean and atmosphere (buried) through diagenetic reactions. During the late Paleozoic Ice Age, meteoric diagenesis could reasonably account for $\sim 1.4\text{\textperthousand}$ increase in global DIC. These findings improve biogeochemical models that have difficulties reconciling the high $\delta^{13}\text{C}$ of the ocean at this time, resulting in lower atmospheric oxygen estimates in GEOCARBSULF [Berner, 2006], and more accurate $\delta^{13}\text{C}$ predictions in COPSE [Bergman et al., 2004].

Acknowledgments

B.D., A.C.M., and J.A.H. were supported by the Scott Vertebrate Fund and Princeton University. Jeremy Caves, Akshay Mehra, Alliya Akhtar, Lily Adler, Yuem Park, and newTom Birren provided assistance in the field. We thank the Nevada BLM and San Andres National Wildlife Refuge for sampling and camping access in restricted areas. This paper benefited greatly from discussions with Christian Bjerrum, Jon M. Husson, and Anne-Sofie Ahm. The USGS Core Research Center provided access to two cores through the Leadville Limestone. Alison Campion, Collin Edwards, Natalie Saenz, Yuem Park, Julia Wilcots, Leah Nelson, Katherine McLellan, Anna Erkalova, and Josh Zoellmer helped prepare samples for isotopic analysis at Princeton University. New literature compiled $\delta^{13}\text{C}$ data for the Carboniferous are included online as a supporting information table file.

References

- Algeo, T. J., and S. E. Scheckler (1998), Terrestrial-marine teleconnections in the Devonian: Links between the evolution of land plants, weathering processes, and marine anoxic events, *Philos. Trans. R. Soc. London B*, 353(1365), 113–130.
- Bachtel, S. L., and S. L. Dorobek (1998), Mississippian carbonate ramp-to-basin transitions in south-central New Mexico: Sequence stratigraphic response to progressively steepening outer-ramp profiles, *J. Sediment. Res.*, 68(6), 1189–1200.
- Baldau, J. (1992), *Middle Eocene Through Early Miocene Diatom Floral Turnover*, pp. 310–326, Princeton Univ. Press, Princeton, N. J.
- Batt, L., I. Montañez, P. Isaacson, M. Pope, S. Butts, and J. Abplanalp (2007), Multi-carbonate component reconstruction of Mid-Carboniferous (Chesterian) seawater [delta] ^{13}C , *Palaeogeogr. Palaeoclimatol. Palaeoecol.*, 256(3-4), 298–318.
- Belcher, C. M., J. M. Yearsley, R. M. Hadden, J. C. McElwain, and G. Rein (2010), Baseline intrinsic flammability of earth's ecosystems estimated from paleoatmospheric oxygen over the past 350 million years, *Proc. Natl. Acad. Sci. U. S. A.*, 107(52), 22,448–22,453.
- Bergman, N. M., T. M. Lenton, and A. J. Watson (2004), COPSE: A new model of biogeochemical cycling over Phanerozoic time, *Am. J. Sci.*, 304(5), 397–437.
- Berner, R. A. (2006), GEOCARBSULF: A combined model for Phanerozoic atmospheric O_2 and CO_2 , *Geochim. Cosmochim. Acta*, 70(23), 5653–5664.
- Bishop, J. W., I. P. Montañez, E. L. Gulbranson, and P. L. Brenckle (2009), The onset of Mid-Carboniferous glacio-eustasy: Sedimentologic and diagenetic constraints, Arrow Canyon, Nevada, *Palaeogeogr. Palaeoclimatol. Palaeoecol.*, 276(1), 217–243.
- Bishop, J. W., I. P. Montañez, and D. A. Osleger (2010), Dynamic Carboniferous climate change, Arrow Canyon, Nevada, *Geosphere*, 6(1), 1–34.
- Bond, G. C., N. Christie-Blick, M. A. Kominz, and W. J. Devlin (1985), An early Cambrian rift to post-rift transition in the cordillera of western North America, *Nature*, 315, 742–746.
- Brand, U., G. Jiang, K. Azmy, J. Bishop, and I. P. Montañez (2012), Diagenetic evaluation of a Pennsylvanian carbonate succession (Bird Spring Formation, Arrow Canyon, Nevada, U.S.A.)—I: Brachiopod and whole rock comparison, *Chem. Geol.*, 308–309, 26–39.
- Bruckschen, P., S. Oesmann, and J. Veizer (1999), Isotope stratigraphy of the European Carboniferous: Proxy signals for ocean chemistry, climate and tectonics, *Chem. Geol.*, 161(1-3), 127–163.
- Budd, D. A. (1988), Aragonite-to-calcite transformation during fresh-water diagenesis of carbonates: Insights from pore-water chemistry, *Geol. Soc. Am. Bull.*, 100(8), 1260–1270.
- Buggisch, W., M. M. Joachimski, G. Sevastopulo, and J. R. Morrow (2008), Mississippian delta C-13(carb) and conodont apatite delta O-18 records—Their relation to the late Palaeozoic glaciation, *Palaeogeogr. Palaeoclimatol. Palaeoecol.*, 268(3), 273–292.
- Buggisch, W., X. Wang, A. S. Alekseev, and M. M. Joachimski (2011), Carboniferous-Permian carbon isotope stratigraphy of successions from China (Yangtze platform), USA (Kansas) and Russia (Moscow basin and Urals), *Palaeogeogr. Palaeoclimatol. Palaeoecol.*, 301(1-4), 18–38.
- Cagliari, J., E. L. C. Lavina, R. P. Philipp, F. M. W. Tognoli, M. A. S. Basei, and U. F. Faccini (2014), New Sakmarian ages for the Rio Bonito formation (Paraná Basin, southern Brazil) based on LA-ICP-MS U-Pb radiometric dating of zircons crystals, *J. South Am. Earth Sci.*, 56, 265–277.
- Campion, A., and A. C. Maloof (2015), Far-field record of the late Paleozoic ice age in northern England, poster presented at Northeastern Geobiology Symposium, Princeton, N. J.
- Caputo, M., J. Melo, M. Streel, and J. Isbell (2008), Late Devonian and Early Carboniferous glacial records of South America, *Spec. Pap. Geol. Soc. Am.*, 441, 161–173, doi:10.1130/2008.2441(11).
- Cleal, C. J., and B. A. Thomas (2005), Palaeozoic tropical rainforests and their effect on global climates: Is the past the key to the present?, *Geobiology*, 3(1), 13–31.
- Davydov, V., D. Korn, and M. Schmitz (2012), The Carboniferous period in *The Geologic Time Scale*, edited by F. Gradstein et al., pp. 603–651, Elsevier, Boston, Mass.
- Dickinson, W. R. (2006), Geotectonic evolution of the Great Basin, *Geosphere*, 2(7), 353–368.
- Domeier, M., R. Van der Voo, and T. H. Torsvik (2012), Paleomagnetism and Pangea: The road to reconciliation, *Tectonophysics*, 514, 14–43.
- Dunham, R. (1962), Classification of carbonate rocks according to depositional texture, *Mem. Am. Assoc. Pet. Geol.*, 1, 108–121.
- Dyer, B., and A. C. Maloof (2015), Physical and chemical stratigraphy suggest small or absent glacioeustatic variation during formation of the Paradox Basin cyclothsems, *Earth Planet. Sci. Lett.*, 419, 63–70.
- Elrick, M., and L. Scott (2010), Carbon and oxygen isotope evidence for high-frequency (104–105 yr) and my-scale glacio-eustasy in middle Pennsylvanian cyclic carbonates (Gray Mesa formation), central New Mexico, *Palaeogeogr. Palaeoclimatol. Palaeoecol.*, 285(3-4), 307–320.
- Emiliani, C. (1995), Two revolutions in the earth sciences, *Terra Nova*, 7(6), 587–597.
- Eros, J., I. Montañez, D. Osleger, V. Davydov, T. Nemyrovska, V. Poletaev, and M. Zhykalyak (2012), Sequence stratigraphy and onlap history of the Donets Basin, Ukraine: Insight into Carboniferous icehouse dynamics, *Palaeogeogr. Palaeoclimatol. Palaeoecol.*, 313–314, 1–25.
- Fielding, C. R., and T. D. Frank (2015), Onset of the glacioeustatic signal recording late Palaeozoic Gondwanan ice growth: New data from palaeotropical East Fife, Scotland, *Palaeogeogr. Palaeoclimatol. Palaeoecol.*, 426, 121–138.
- Fielding, C. R., T. D. Frank, and J. L. Isbell (2008), The late Paleozoic ice age—a review of current understanding and synthesis of global climate patterns, *Spec. Pap. Geol. Soc. Am.*, 441, 343–354.
- Folk, R. L., H. H. Roberts, and C. H. Moore (1973), Black phytokarst from hell, Cayman Islands, British West Indies, *Geol. Soc. Am. Bull.*, 84(7), 2351–2360.

- Fouret, K. L. (1996), Depositional and diagenetic environments of the Mississippian Leadville limestone at Lisbon field, Utah, in *Geology and Resources of the Paradox Basin Utah Geologic Association Guidebook 25*, edited by A. C. Huffman, W. R. Lund, and L. H. Godwin, pp. 129–138, Utah Geol. Assoc., Salt Lake City, Utah.
- Frank, T. D., K. C. Lohmann, and W. J. Meyers (1995), Chronostratigraphic significance of cathodoluminescence zoning in syntectonic cement: Mississippian Lake Valley Formation, New Mexico, *Sediment. Geol.*, 105(1), 29–50.
- Glasspool, I. J., and A. C. Scott (2010), Phanerozoic concentrations of atmospheric oxygen reconstructed from sedimentary charcoal, *Nat. Geosci.*, 3(9), 627–630.
- Gross, M. G. (1964), Variations in the O^{18}/O^{16} and C^{13}/C^{12} ratios of diagenetically altered limestones in the Bermuda islands, *J. Geol.*, 72, 170–194.
- Halverson, G. P., P. F. Hoffman, D. P. Schrag, and A. J. Kaufman (2002), A major perturbation of the carbon cycle before the Ghaub glaciation (Neoproterozoic) in Namibia: Prelude to snowball earth?, *Geochem. Geophys. Geosyst.*, 3(6), 1–24.
- Hoffman, P., and A. Maloof (2003), Comment on: A complex microbiota from snowball earth times: Microfossils from the Neoproterozoic Kingstone Peak Formation, Death Valley, USA, *Proc. Natl. Acad. Sci. U. S. A.*, 100, 4399–4404.
- Hughes, T. J., and G. H. Denton (1981), *The Last Great Ice Sheets*, John Wiley, N. Y.
- Huybers, P. (2006), Early Pleistocene glacial cycles and the integrated summer insolation forcing, *Science*, 313(5786), 508–511.
- Imbrie, J., and K. P. Imbrie (1986), *Ice Ages: Solving the Mystery*, Harvard Univ. Press, Cambridge, Mass.
- Isaacson, P., E. Diaz-Martinez, G. Grader, J. Kalvoda, O. Babek, and F. Devuyst (2008), Late Devonian–earliest Mississippian glaciation in Gondwanaland and its biogeographic consequences, *Palaeogeogr. Palaeoclimatol. Palaeoecol.*, 268(3), 126–142.
- Isbell, J., M. Miller, K. Wolfe, and P. Lenaker (2003), Timing of late Paleozoic glaciation in Gondwana: Was glaciation responsible for the development of northern hemisphere cycloths, in *Extreme Depositional Environments: Mega End Members in Geologic Time*, *Geol. Soc. Spec. Publ.*, 370, 5–24.
- Jones, D. S., R. C. Creel, B. Rios, and D. P. S. Ramos (2015), Chemostratigraphy of an Ordovician–Silurian carbonate platform: $\delta^{13}C$ records below glacioeustatic exposure surfaces, *Geology*, 43(1), 59–62.
- Kellogg, D. E., and T. B. Kellogg (1996), Diatoms in south pole ice: Implications for eolian contamination of sirius group deposits, *Geology*, 24(2), 115–118.
- Knauth, L. P., and M. J. Kennedy (2009), The late Precambrian greening of the earth, *Nature*, 460(7256), 728–732.
- Koch, J. T., T. D. Frank, and T. P. Bulling (2014), Stable-isotope chemostratigraphy as a tool to correlate complex Mississippian marine carbonate facies of the Anadarko shelf, Oklahoma and Kansas, *AAPG Bull.*, 98(6), 1071–1090.
- Kump, L. R., and M. A. Arthur (1999), Interpreting carbon-isotope excursions: Carbonates and organic matter, *Chem. Geol.*, 161(1), 181–198.
- Lane, H. (1999), The IUGS boundary in the middle of the Carboniferous: Arrow Canyon, Nevada, USA, *Episodes*, 22(4), 272–283.
- Lohmann, K. C. (1988), Geochemical patterns of meteoric diagenetic systems and their application to studies of paleokarst, in *Paleokarst*, pp. 58–80, Springer, N. Y.
- Meyers, W. J. (1985), Isotope geochemistry of regionally extensive calcite cement zones and marine components in Mississippian limestones, New Mexico, in *Carbonate Cement*, edited by N. Schneidermann and P. Harris, *Spec. Publ. Soc. Econ. Paleontol. Mineral.*, 36, 223–240.
- Mii, H., E. Grossman, and T. Yancey (1999), Carboniferous isotope stratigraphies of North America: Implications for Carboniferous paleoceanography and Mississippian glaciation, *Geol. Soc. Am. Bull.*, 111(7), 960–973.
- Miller, K. G., M. A. Kominz, J. V. Browning, J. D. Wright, G. S. Mountain, M. E. Katz, P. J. Sugarman, B. S. Cramer, N. Christie-Blick, and S. F. Pekar (2005), The Phanerozoic record of global sea-level change, *Science*, 310(5752), 1293–1298.
- Montañez, I. P., and C. J. Poulsen (2013), The late Paleozoic ice age: An evolving paradigm, *Annu. Rev. Earth Planet. Sci.*, 41(1), 629–656.
- Nemyrovska, T., R. Wagner, C. W. Prins, and I. Montañez (2011), Conodont faunas across the mid-Carboniferous boundary from the Barciliante Formation at La Lastra (Palentian Zone, Cantabrian Mountains, Northwest Spain); geological setting, sedimentological characters and faunal descriptions, *Scr. Geol.*, 143, 127–183.
- Peters, S. E. (2008), Environmental determinants of extinction selectivity in the fossil record, *Nature*, 454(7204), 626–629.
- Phillips, T. L., and R. A. Peppers (1984), Changing patterns of Pennsylvanian coal-swamp vegetation and implications of climatic control on coal occurrence, *Int. J. Coal Geol.*, 3(3), 205–255.
- Proske, A. (2013), Conodont biostratigraphy of lower Mississippian strata, San Andres mountains, New Mexico, PhD thesis, Tex. Tech Univ., Lubbock.
- Ronchi, P., A. Ortenzi, O. Borromeo, M. Claps, and W. G. Zempolich (2010), Depositional setting and diagenetic processes and their impact on the reservoir quality in the late Viséan–Bashkirian Kashagan carbonate platform (pre-Caspian basin, Kazakhstan), *AAPG Bull.*, 94(9), 1313–1348.
- Ronov, A. (1982), The Earth's sedimentary shell (quantitative patterns of its structure, compositions, and evolution), *Int. Geol. Rev.*, 24(11), 1313–1365.
- Rose, C. V., N. L. Swanson-Hysell, J. M. Husson, L. N. Poppick, J. M. Cottle, B. Schoene, and A. C. Maloof (2012), Constraints on the origin and relative timing of the Trezona $\delta^{13}C$ anomaly below the end-Cryogenian glaciation, *Earth Planet. Sci. Lett.*, 319, 241–250.
- Saltzman, M. (2002), Carbon and oxygen isotope stratigraphy of the lower Mississippian (Kinderhookian–lower Osagean), western United States: Implications for seawater chemistry and glaciation, *Geol. Soc. Am. Bull.*, 114(1), 96–108.
- Saltzman, M. (2005), Phosphorus, nitrogen, and the redox evolution of the Paleozoic oceans, *Geology*, 33(7), 573–576.
- Sando, W. J. (1988), Madison Limestone (Mississippian) Paleokarst: A geologic synthesis, in *Paleokarst*, pp. 256–277, Springer, N. Y.
- Sanz López, J., S. Blanco Ferrera, S. García López, and L. C. Sánchez de Posada (2006), The mid-Carboniferous boundary in northern Spain: Difficulties for correlation of the global stratotype section and point, *Rivista Ital. Paleontol. Stratigr.*, 112(1), 3–22.
- Saunders, W., and W. Ramsbottom (1986), The mid-Carboniferous eustatic event, *Geology*, 14(3), 208–212.
- Schrag, D. P., J. A. Higgins, F. A. Macdonald, and D. T. Johnston (2013), Authigenic carbonate and the history of the global carbon cycle, *Science*, 339(6119), 540–543.
- Scott, A., and I. Glasspool (2006), The diversification of paleozoic fire systems and fluctuations in atmospheric oxygen concentration, *Proc. Natl. Acad. Sci. U. S. A.*, 103(29), 10,861–10,865.
- Stollhofen, H., M. Werner, I. Stanstreet, R. Armstrong, C. Fielding, T. Frank, and J. Isbell (2008), Single-zircon U-Pb dating of Carboniferous–Permian tuffs, Namibia, and the intercontinental deglaciation cycle framework, in *Resolving the Late Paleozoic Ice Age in Time and Space*, *Geol. Soc. Spec. Publ.*, 441, 83–96.
- Swart, P., and M. Kennedy (2012), Does the global stratigraphic reproducibility of $\delta^{13}C$ in Neoproterozoic carbonates require a marine origin? A Pliocene–Pleistocene comparison, *Geology*, 40(1), 87–90.
- Swart, P. K., and G. Eberli (2005), The nature of the $\delta^{13}C$ of periplatform sediments: Implications for stratigraphy and the global carbon cycle, *Sediment. Geol.*, 175(1), 115–129.

- Vacher, H., T. Bengtsson, and L. Plummer (1990), Hydrology of meteoric diagenesis: Residence time of meteoric ground water in island fresh-water lenses with application to aragonite-calcite stabilization rate in Bermuda, *Geol. Soc. Am. Bull.*, 102(2), 223–232.
- Van Andel, T. H., G. R. Heath, and T. C. Moore (1975), Cenozoic history and paleoceanography of the central equatorial pacific ocean a regional synthesis of deep sea drilling project data, *Geol. Soc. Am. Mem.*, 143, 1–223.
- Walker, L. J., B. H. Wilkinson, and L. C. Ivany (2002), Continental drift and Phanerozoic carbonate accumulation in shallow-shelf and deep-marine settings, *J. Geol.*, 110(1), 75–87.
- Zachos, J., M. Pagani, L. Sloan, E. Thomas, and K. Billups (2001), Trends, rhythms, and aberrations in global climate 65 ma to present, *Science*, 292(5517), 686–693.
- Zhao, M.-Y., and Y.-F. Zheng (2014), Marine carbonate records of terrigenous input into paleotethyan seawater: Geochemical constraints from Carboniferous limestones, *Geochim. Cosmochim. Acta*, 141, 508–531.